Electronic Supplementary Information

In situ Anchor of $Na_2Ti_3O_7$ in Nitrogen-Rich Carbon Hollow Red Cells as 0D-3D Hierarchical Electrode materials for Efficient Electrochemical Desalination

Yingying Zhang, Xiaogeng Feng, Yuejiao Wang, Weijun Shan, Zhenning Lou, Ying Xiong[*]

College of Chemistry, Key Laboratory of Rare-scattered Elements of Liaoning
Province, Liaoning University, Shenyang 110036, P. R. China
E-mail:xiongying_1977@hotmail.com

1. Experimental Section

1.1. Chemicals

Amino-terephthalic acid (NH_2-H_2BDC), tannin acid (TN), and sodium hydroxide (NaOH), tetra-n-butyl titanate (TBOT), *N,N*-dimethylformamide (DMF), N-methyl-2-pyrrolidone (NMP), anhydrous methanol (MeOH), and P25 (TiO_2 with anatase phases) were purchased from Sinopharm Chemical Reagent Co. Ltd. (China) and used without further purification.

1.2. Synthesis of NH_2-MIL-125 composite materials

First, 1.0 g NH_2-H_2BDC and 0.5 mL TBOT were added to the mixture of 45 mL DMF and 5 mL MeOH and continually stirred for 30 min. Then, the mixture was transferred into 100 mL autoclave and maintained at 150 °C for 24 h. After cooling down to room temperature, the product was centrifugated, washed three times with MeOH and DMF for 3 times, as well as dried at 60 °C.

1.3. Synthesis of HRBC-MOF-x

HRBC-MOF-x were obtained by a selective protection strategy. Typically, 0.05 g of NH_2-MIL-125 cake were dispersed in 50 mL of aqueous solution containing 0.10 g of tannic acid. After stirring for 20 min, the mixture was moved to a Teflon-lined pressure vessel (100 mL inner volume) and reacted at 150 °C for 0, 30, 60 90 min, the corresponding products were designated as NH_2-MIL-125, HRBC-MOF-30, HRBC-MOF-60 and HRBC-MOF-90. Meanwhile, NH_2-MIL-125-60 was obtained by reacting NH_2-MIL-125 at 150 °C for 60 min.

1.4. Synthesis of HR-NTO/N-C-x and NTO-60

Synthesis of HRBC-NTO/N-C-x and NTO-60: The as-prepared NH_2-MIL-125, HRBC-MOF-30, HRBC-MOF-60 and HRBC-MOF-90 were annealed at 600 °C for 2 h under N_2 atmosphere and alkalized in 0.8 mol L^{-1} NaOH solution at 140 °C for 6 h. Then, the products were collected by centrifugation with water. The corresponding products were assigned as HRBC-NTO/N-C-0, HRBC-NTO/N-C-30, HRBC-NTO/N-C-60, and HRBC-NTO/N-C-90. In addition, NH_2-MIL-125-60 was annealed at 600 °C for 2 h under N_2 atmosphere and alkalized in 0.8 mol L^{-1} NaOH solution at 140 °C for 6 h. The NTO-60 particles were collected by centrifugation, and washed several times with water.

1.5. Synthesis of Ag@rGO composite materials[1]

Synthesis of graphene oxide (GO): Typically, 2 g graphite powder and 1 g $NaNO_3$ were added into a beaker with 50 mL H_2SO_4 successively. After the beaker was continuously stirred under the ice bath for 15 minutes, 5 g of $KMnO_4$ was slowly added and kept stirring under the ice bath for 2 hours. After the beaker rose to room temperature, it kept stirring under 40 °C for 2 hours. Then 100 mL DI was added into the beaker and continue the reaction for 30 minutes. Afterwards, 100 mL boiled DI was also added into the beaker and kept stirring for 10 minutes, following moderate hydrogen peroxide (H_2O_2) was added and stood for several hours. The precipitate was washed with DI by using centrifuge until the PH equals to 7. Finally, the precipitate was performed ultrasound and centrifuged for three times to obtain GO flakes.

Synthesis of Ag@rGO: 0.0472 g silver nitrate ($AgNO_3$) was added into a beaker with 60 mL GO (~1 $mg \cdot L^{-1}$) and kept ultrasound for 1 hour. Afterwards, a beaker with 15 ml sodium hydroxide (NaOH, 4 $mol \cdot L^{-1}$) was kept stirring under 85 ℃ and accompanied by adding the solution above drop by drop. Finally, the beaker was kept stirring for 30 minutes. The black precipitate was washed with DI by using centrifuge until the PH equals to 7.

2.1. Structural characterization

The characteristic peaks of the functional groups presented in the samples before and after modifying were recorded using Fourier transform infrared spectroscopy (FT-IR) by KBr pellet method within the scope of 400 ~ 4000 cm^{-1}. The X-ray diffraction analysis (XRD) of the as-prepared materials at 2θ angles were performed on a Bruker D8 Advance diffractometer using Cu-Kα radiation. The microstructures and porosity of the products were characterized by a JEM-2100F (JEOL, Japan) transmission electron microscopy (TEM), and by a SU8010 (Hitachi, Japan) field emission scanning electron microscope (SEM). The properties of the wall structure were measured by N_2 adsorption-desorption at 77 K employing a Tristar 3020 volumetric adsorption analyzer (Norcross, GA), and outgassed at a relative pressure (P/P_0) of 0.005 under 373 K for 4 h. The specific surface area and the pore diameter distribution were calculated through the Brunauer-Emmett-Teller (BET) method and the Barrett-Joyner-Halenda (BJH) method. X-ray photoelectron spectroscopic (XPS) analysis was carried out on an X-ray photoelectron spectrometer (thermo ESCALAB 250) equipped with a hemispherical electron analyzer (pass energy of 100 eV) and an Al Kα (hv = 1486.6 eV) X-ray source. The binding energies (BE) were referenced to the adventitious C 1s peak (284.6 eV) which was used as an internal standard to take into account charging effects. Meanwhile, XPS spectra of the samples were further deconvoluted into one or several narrow-scan spectra of the C 1s, O 1s, Ti 2p, Na 1s and N 1s by using the software of XPS Peak (Version 4.1). The conductivities of NaCl solutions were tested by a conductivity meter (DDSJ-308F, Leici).

3.1. Electrochemical characterization

To prepare the electrode, 70% active materials, 10% carbon black, and 20% PVDF were mixed. Secondly, the NMP solution was placed into the mixture and ground until it becomes homogeneous slurry. The prepared slurry was painted on a graphite sheet and dried at 80 °C overnight for electrochemical and/or desalination battery tests. Finally, the approximate active mass loading for electrodes was around 0.5 mg·cm^2 and the size was 9 cm^2.

All electrochemical performance of NTO-60 and HRBC-NTO/N-C-x was conducted in 2 mol·L^{-1} NaCl solution using CHI760E electrochemical workstation (Shanghai, Chenhua, China) in a three-electrode mode. The three-electrode system was composed of Ag/AgCl reference electrode, platinum sheet (1 cm^2) counter electrode and graphite plate (1 cm^2) loaded with the samples working electrode. Cyclic voltammetry was conducted over the potential window from 0 to 0.9 V under various scanning speeds (0.05, 2, 5, 10, and 20 $mV \cdot s^{-1}$). Electrochemical impedance spectroscopy (EIS) for the samples was carried out at open-circuit potential by setting the amplitude to 5 mV and the frequency range from 1 M Hz to 0.1 Hz. The GCD was measured by setting the upper potential limit at 1.0 V vs. Ag/AgCl at different current density of 1, 2, 3, 4, and 5 $A \cdot g^{-1}$. The specific capacitance (SC, $F \cdot g^{-1}$) can be obtained from the GCD curves according to the following equation:

$$SC = Imt/\Delta V \tag{S1}$$

Where I_m is the response current (A), m is the mass of activated materials (g), t is the discharge time (s) and ΔV is the potential change (V) during the discharge.

3.2. Electrochemical deionization tests

The measurement of the desalination battery was conducted via a typical set-up as depicted in Fig.S5C. The desalination battery cell includes NTO-60 or HRBC-NTO/N-C-x cathode, spacer, cation exchange membrane (CEM), Ag@rGO anode, and anion exchange membrane (AEM). The effective area of active material for electrode size was 3 cm × 3 cm. In the batch experiments, 35 mL NaCl solution with different concentrations (100, 200, 300, 400 and 500 $mg \cdot L^{-1}$) through the cell by a peristaltic pump with a flow rate (12.5, 25, and 50 $mL \cdot min^{-1}$). In addition, we were also discussing the effect of applied voltages (from 1.0 to 1.4 V) on the desalination performance. The conductivity of the solution was continuously monitored and recorded every 60 s by a conductivity meter (DDSJ-308F, Leici). The desalination performance including desalination capacity (SAC, mg·g^{-1}), charge efficiency (Λ), ion adsorption rate (IAR, mg·g^{-1}·min^{-1}) was evaluated based on the following equations:

$$SAC = (C_0 - C_t) \times V / m_t \tag{S2}$$

$$\Lambda = SAC \times F / C \tag{S3}$$

$$IAR = SAC / t \tag{S4}$$

Where C_0 (mg·L^{-1}) and C_t (mg·L^{-1}) is initial and final NaCl solution concentrations, respectively, m_t (g) is the total mass of active materials, V is volume of NaCl solution, F is the Faraday constant (96485 C·mol^{-1}), C (charge, C·g^{-1}) is obtained by integrating the corresponding current.

Captions

Fig.S1. Comparison of packing of spherical hollow particles and red cells-like hollow particles.

Fig.S2. FTIR spectrum of TN, NH_2-MIL-125, HRBC-MOF-x, and NH_2-MIL-125-60 (a). XRD spectrum of NH_2-MIL-125 and HRBC-MOF-x (b).

Fig.S3. SEM images of NH_2-MIL-125-60 (a) and NTO-60 (b).

Fig.S4. TEM (a,b) and HRTEM (c,d) images of HRBC-NTO/N-C-60.

Fig.S5. GCD curves of NTO-60 (a), HRBC-NTO/N-C-0 (b), HRBC-NTO/N-C-30 (c), HRBC-NTO/N-C-60 (d), and HRBC-NTO/N-C-90 (e). CV curves of HRBC-NTO/N-C-60 (f) at various scanning speeds.

Fig.S6. Normalized contribution ratio of capacitance (yellow) and diffusion controlled (blue) processes of HRBC-NTO/N-C-60 (a). CV curves of Ag@rGO at the scanning speed of 100 $mV \cdot s^{-1}$ (b).The structure of the desalination battery model (c). Desalination performance of all samples in a 200 $mg \cdot L^{-1}$ NaCl solution at 1.4 V with a flow rate of 25 $mL \cdot min^{-1}$ (d).

Fig.S7. The effect of voltage and flow rate on the desalination performance of HRBC-NTO/N-C-60 in a 200 $mg \cdot L^{-1}$ NaCl solution (a-c).

Fig.S8. The effect of voltage and flow rate on the *SAR* of HRBC-NTO/N-C-60 in a 200 $mg \cdot L^{-1}$ NaCl solution (a) Conductivity transients of the desalination system at different initial concentration of NaCl solution (b-f).

Fig. S9. SEM image of HRBC-NTO/N-C-60 (a) after cycling, and SEM image of Ag@rGO before (b) and after (c).

Tab.S1. Desalination performance of different electrode materials used for CDI process.

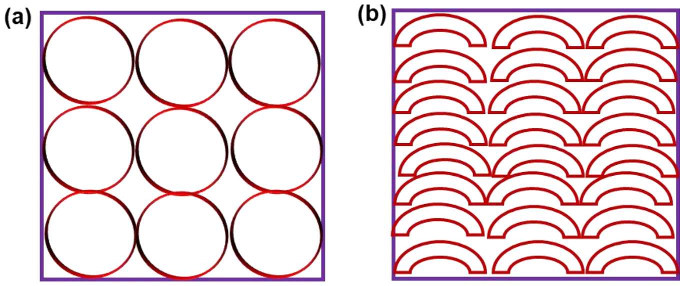

Fig.S1. Comparison of packing of spherical hollow particles and red cells-like hollow particles.

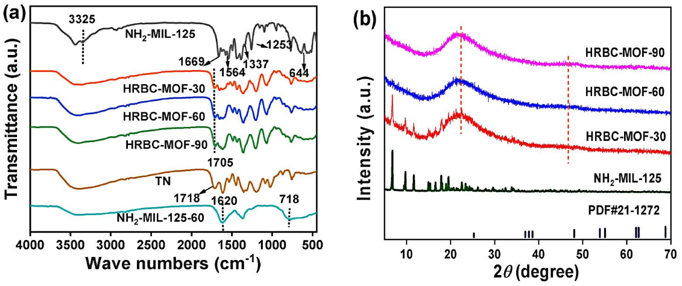

Fig.S2. FTIR spectrum of PT, NH$_2$-MIL-125, HRBC-MOF-x, and NH$_2$-MIL-125-60 (a). XRD spectrum of NH$_2$-MIL-125 and HRBC-MOF-x (b).

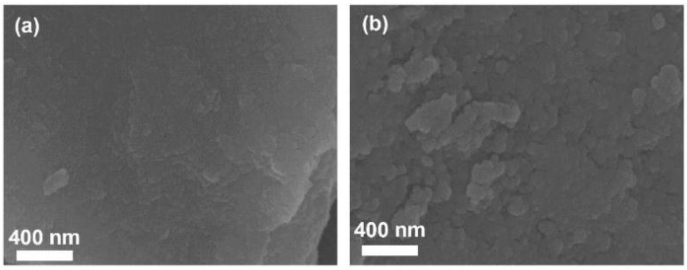

Fig.S3. SEM images of NH$_2$-MIL-125-60 (a) and NTO-60 (b).

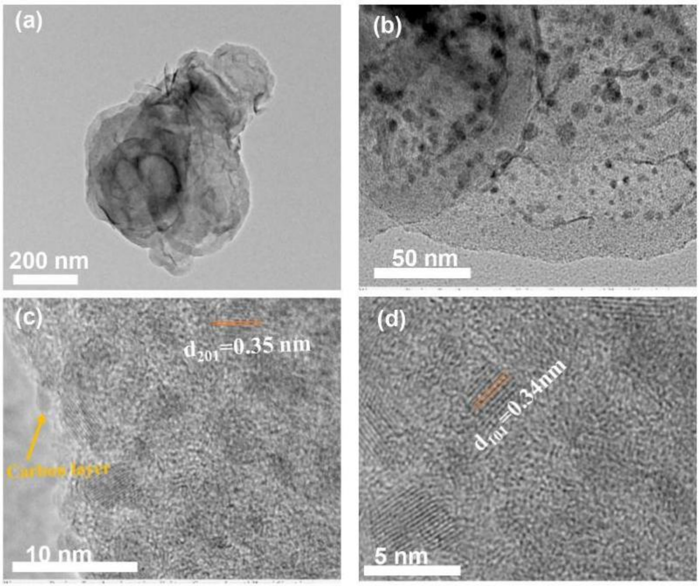

Fig.S4. TEM (a,b) and HRTEM (c,d) images of HRBC-NTO/N-C-60.

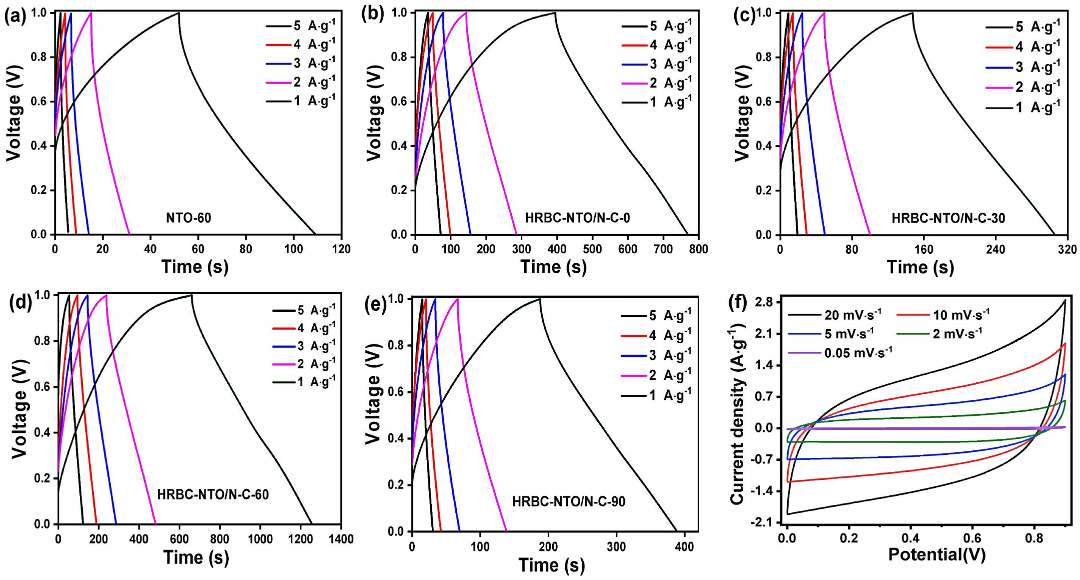

Fig.S5. GCD curves of NTO-60 (a), HRBC-NTO/N-C-0 (b), HRBC-NTO/N-C-30 (c), HRBC-NTO/N-C-60 (d), and HRBC-NTO/N-C-90 (e). CV curves of HRBC-NTO/N-C-60 (f) at various scanning speeds.

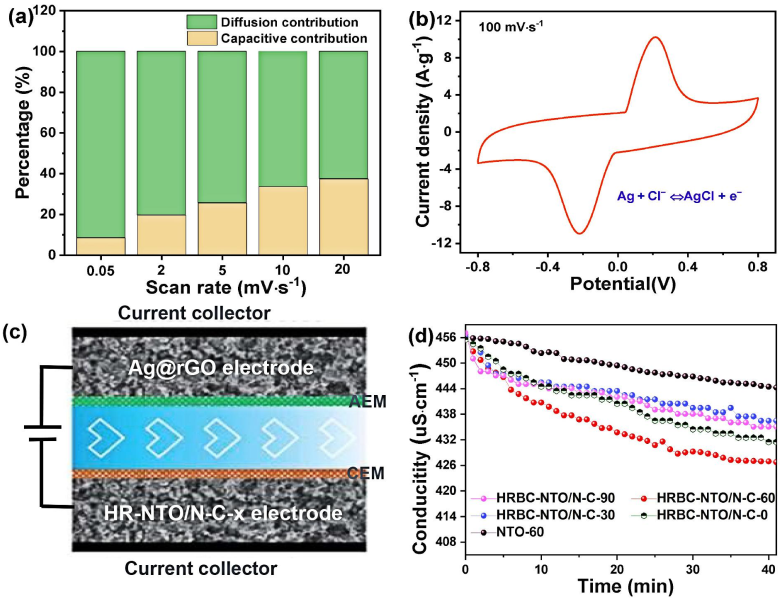

Fig.S6. Normalized contribution ratio of capacitance (yellow) and diffusion controlled (blue) processes of HRBC-NTO/N-C-60 (a). CV curves of Ag@rGO at the scanning speed of 100 mV·s^{-1} (b).The structure of the desalination battery model (c). Desalination performance of all samples in a 200 mg·L^{-1} NaCl solution at 1.4 V with a flow rate of 25 mL·min^{-1} (d).

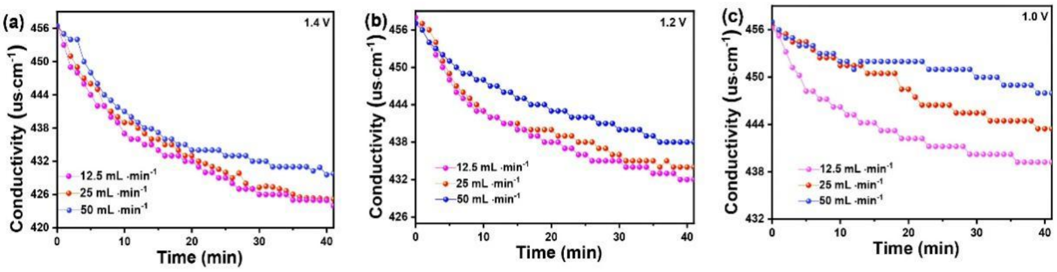

Fig.S7. The effect of voltage and flow rate on the desalination performance of HRBC-NTO/N-C-60 in a 200 mg·L^{-1} NaCl solution (a-c).

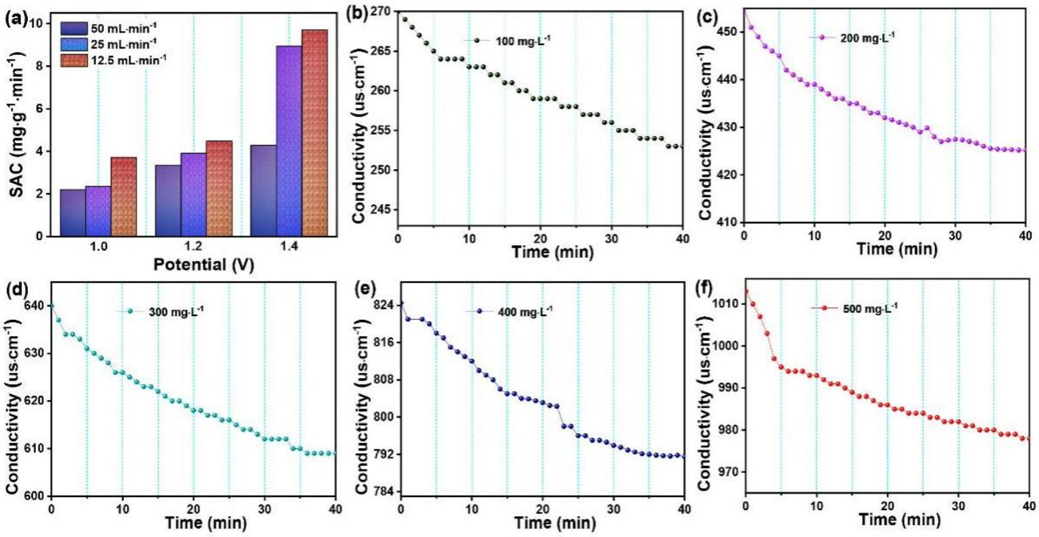

Fig.S8. The effect of voltage and flow rate on the *SAR* of HRBC-NTO/N-C-60 in a 200 mg·L^{-1} NaCl solution (a) Conductivity transients of the desalination system at different initial concentration of NaCl solution (b-f).

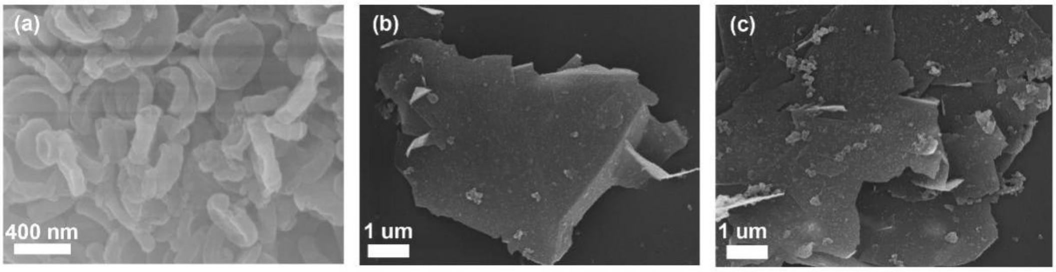

Fig. S9. SEM image of HRBC-NTO/N-C-60 (a) after cycling, and SEM image of Ag@rGO before (b) and after (c) cycling.

Tab.S1. Desalination performance of different electrode materials used for CDI process.

Materials	NaCl concentration $(mg\cdot L^{-1})$	Operation potential (V)	Maximum Desalination rate $(mg\cdot g^{-1}\cdot min^{-1})$	Time (min)	Desalination capacity $(mg\cdot L^{-1})$	Ref.
N-doped porous carbon	500	1.2	~ 1.1	60	21.1	S2
Fe, N-doped carbon	350	1.2	~ 6	30	40.7	S3
$Na_{0.71}CoO_2$	500	1.4	3	40	31	S4
AC@$NaMnO_2$	500	1.2	5.7	10	32.7	S5
C@NTO	500	1.4	~ 1	120	49.91	S6
rGO@NTO	250	1.4	~1	60	41.8	S7
MnO_2/AC	2000	1.2	2.95	10	25.7	S8
Co-Fe-LDH	600	1.2	~ 1	120	34.2	S9
3D NTO/N-C-2	1000	1.4	3.9	60	59.3	S10
N, Ti-dopede carbon	500	1.2	3.53	30	13.89	S11
Carbon cages	1000	1.2	~2	35	47.2	S12
N-doped 3D nanofibrous	250	1.6	5.6	30	44.8	S13
SbH_3	135	1.2	~ 3	60	31.4	S14
mPDA/MXene	1000	1.5	1.27	30	37.72	S15
$W_{18}O_{49}/Ti_3C_2$	500	1.2	~7	30	29.95	S16
Ni-CuPBA/CNTs	500	1.4	-	25	34.3	S17
Porous carbon	585	1.2	1.2	30	35.6	S18
MnO_2	877	1.2	~6.6	15	27.8	S19
Ordered porous carbon	500	1.2	3.2	60	23.6	S20
MOF/PPy	584	1.2	~2	30	11.34	S21
Nitrogen-doped MXene	5000	1.2	-	10	43.5	S22
3DGA-OP	50	1.2	~1	120	14.4	S23
MoS_2/rGO	300	1.4	-	30	34.2	S24
ZIF-67/CNTs	1170	1.2	-	30	16.90	S25
Carbon nanosheets	500	1.2	-	50	30.1	S26
TiO_2/C@NMC	500	1.2	-	40	27.73	S27
Ti_3C_2Tx shell	5000	1.6	~1	60	53	S28
MnV_2O_6@rGO	1000	1.4	-	120	49.3	S29

NPC/rGO	1000	1.2	-	30	39.34	S30
HRBC-NTO/N-C-60	200	1.2	3.7	40	53.6	This work
HRBC-NTO/N-C-60	200	1.4	8.9	40	66.8	This work

References

S1. Z. H. Yue, Y. L. Ma, J. W. Zhang and H. B. Li, *J. Mater. Chem. A*, 2019, **7**, 16892-16901.

S2. M. Z. Zong, S. L. Huo, Y. Liu, X. L. Zhang and K. X. Li, *Sep. Purif. Technol.*, 2021, **256**, 117818-117827.

S3. X. T. Xu, J. Tang, Y. V. Kaneti, H. Tan, T. Chen, L. K. Pan, T. Yang, Y. Bando and Y. Yamauchi, *Mater. Horiz.* 2020, **7**, 1404-1412.

S4. Z. Z. Liu, Z. S. Yue and H. B. Li, *Sep. Purif. Technol.*, 2020, **234**, 116090-116100.

S5. S. Y. Wang, G. Wang, X. Che, S. Wang, C. Li, D. Li, Y. Zhang, Q. Dong and J. S. Qiu, *Environ. Sci: Nano*, 2019, **6**, 2379-2388.

S6. Z. S. Yue, T. Gao and H. B. Li, *Desalination*, 2019, **449**, 69-77.

S7. F. Zhou, T. Gao and H. B. Li, *Chem. Eng. J.,* 2018, **343**, 8-15.

S8. Y. Liu, B. Geng, Y. C. Zhang, X. Gao, X. Du, X. Y. Dou, H. G. Zhu and X. Yuan, *Desalination*, 2021, **504**, 114977-114985.

S9. Z. Li, S. Mao, Y. Yang, Z. Sun and R. Zhao, *J Colloid Interf. Sci.*, 2021, **585**, 85-94.

S10. Y. Y. Zhang, K. Yang, H. B. Yu, W. J. Shan, Z. N. Lou and Y. Xiong, *J. Mater. Chem. A*, 2021, **9**, 24374-24386.

S11. T. Gao, Z. Z. Liu and H. B. Li, *Sep.Purif. Technol.*, 2020, **231**, 115918-115926.

S12. S. L. Huo, X. Song, Y. Z. Zhao, W. Ni, H. Wang and K. X. Li, *J. Mater. Chem. A*, 2020, **8**, 19927-19937.

S13. Z. B. Ding, X. T. Xu, J. B. Li, Y. Q. Li, K. Wang, T. Lu, M. S. A. Hossain, M. A. Amin, S. H. Zhang, L. K. Pan and Y. Yamauchi, *Chem. Eng. J.,* 2022, **430**, 133161-133168.

S14. Y. J. Gao, C. Lin, K. Zhang, W. H. Zhou, S. Y. Guo, W. Q. Liu, L. F. Jiang, S. L. Zhang, H. B. Zeng, *Adv. Funct. Mater.,* 2021, **31**, 2102766-2102777.

S15. Q. Li, X. T. Xu, J. R. Guo, J. P. Hill, H. S. Xu, L. X. Xiang, C. Li, Y. Yamauchi and Y. Y. Mai, *Angew. Chem. Int. Ed.,* 2021, **60**, 26528-26534.

S16. J. Liang, J. Q. Yu, W. L. Xing, W. W. Tang, N. Tang and J. Y. Guo, *Chem. Eng. J.,* 2022, **435**, 134922-134934.

S17. J. Q. Guo, Y. Wang, Y. M. Cai, H. Zhang, Y. L. Li and D. X. Liu, *Desalination*, 2022, **528**, 115622-115634.

S18. J. Chen, K. C. Zuo, B. Li, J. H. Hu, W. B. Liu, D. S. Xia, L. Lin, J. J. Liang, X. Y. Li, *Chem. Eng. J.,* 2022,**433**, 133781-133791.

S19. B. W. Byles, D. A. Cullen, K. L. More, E. Pomerantseva, *Nono energy*, 2018, **44**, 476-488.

S20. Y. C. Wu. G. P. Jiang, G. H. Liu, G. Lui, Z. P. Cano, Q. Li, Z. Zhang, A. P. Yu, Z. S. Zhang, Z. W. Chen, *J. Mater. Chem. A,* 2019, **7**, 15633-15639.

S21. Z. M. Wang, X. T. Xu, J. H. Kim, V. Malgras, R. Mo, C. L. Li, Y. Z. Li, H. B. Tan, J. Tang, L. K. Pan, Y. Bando, T. Yang and Y. Yamauchi, *Mater. Horiz.*, 2019, **6**, 1433-1437.

S22. A. Amiri, Y. J. Chen, C. B. Teng and M. Naraghi, *Energy Storage Mater.*, 2020, **25**, 731-739.

S23. Y. H. Zhu, G. J. Zhang, C. Xu and L. Z. Wang, *ACS Appl. Mater. Interfaces*, 2020, **12**, 29706-29716.

S24. L. J. Gao, Q. Dong, S. L. Bai, S. C. Liang, C. Hu and J. S. Qiu, *ACS Sustainable Chem. Eng.,* 2020, **8**, 9690-9697.

S25. X. T. Xu, C. L. Li, C. Wang, L. Ji, Y. V. Kaneti, H. J. Huang, T. Yang, K. C. W. Wu and Y. Yanmauchi, *ACS Sustainable Chem. Eng.*, 2019, **7**, 13949-13954.

S26. S. L. Huo, P. Zhang, M. M. He, W. Zhang, B. L. Liang, M. T. Zhang, H. Wang and K. X. Li, *Green Chem.,* 2021, **23**, 8554-8565.

S27. H. Zhang, C. H. Wang, X. D. Li, J. Xie, X. Yan, J. W. Qi, X. Y. Sun and J. S. Li, *Environ. Sci.: Nano,* 2021, **8**, 3536-3545.

S28. G. J. Zhang, L. H. Wang, R. J. Sa, C. Xu, Z. H. Li and L. Z. Wang, *Environ. Sci.: Nano*, 2022, **9**, 204-213.

S29. E. R. Halabaso, J. W. L. Salvacion, E. P. Kuncoro and R. A. Doong, *Environ. Sci.: Nano*, 2021, **8**, 2844-2854.

S30. J. R. Guo, X. T. Xu, J. P. Hill, L. P. Wang, J. J. Dang, J. J. Dang, Y. Q. Kang, Y. L. Li, W. S. Guan and Y. Yamauchi, *Chem. Sci.*, 2021, **12**, 10334-10340.